

7-1-2016

Impact of a Reverse Delta Type Add-on Device on the Flap-tip Vortex of a Wing

Afaq Altaf

Monash University Malaysia, afaqaltaf@hotmail.com

Tan Boon Thong

Monash University Malaysia, tan.boon.thong@monash.edu

Ashraf Ali Omar

University of Tripoli, aao@aerodept.edu.ly

Waqar Asrar

International Islamic University Malaysia, waqar@iiium.edu.my

Follow this and additional works at: <https://commons.erau.edu/ijaaa>



Part of the [Aerodynamics and Fluid Mechanics Commons](#)

Scholarly Commons Citation

Altaf, A., Thong, T. B., Ali Omar, A., & Asrar, W. (2016). Impact of a Reverse Delta Type Add-on Device on the Flap-tip Vortex of a Wing. *International Journal of Aviation, Aeronautics, and Aerospace*, 3(3). Retrieved from <https://commons.erau.edu/ijaaa/vol3/iss3/12>

This Article is brought to you for free and open access by the Journals at Scholarly Commons. It has been accepted for inclusion in International Journal of Aviation, Aeronautics, and Aerospace by an authorized administrator of Scholarly Commons. For more information, please contact commons@erau.edu.

Impact of a Reverse Delta Type Add-on Device on the Flap-tip Vortex of a Wing

Cover Page Footnote

The authors would like to thank the International Islamic University Malaysia (IIUM) for supporting this work through the Ministry of Science, Technology and Innovation (MOSTI) E-Science research grant no. SF13-001-005. The authors wish to acknowledge the support of the Ministry of Education, Malaysia, through the Fundamental Research Grant Scheme (FRGS/1/2014/TK01/MUSM/02/1).

The study of wake vortices is motivated by the continuous growth of air traffic, with an objective to reduce the current spacing between aircraft while maintaining the same level of safety. The current separation regulations are becoming highly inadequate to cope with future air traffic needs. Vortex flows play an important role in aerodynamic applications such as in the control of wake vortices of large aircraft so as to reduce the danger posed on trailing aircraft (Coustols et al., 2006; Coustols, 2006).

Wake vortices generated by aircraft are an unavoidable consequence of the creation of lift. Factors such as the aircraft's weight, speed, configuration (amount of flaps and slats extension), wingspan, angle of attack and the atmospheric conditions in which the aircraft is being flown determine the intensity of the wake vortices produced by a specific aircraft (Veillette, 2002). Wingtip vortices have been observed to persist for many kilometres (Andrews, 1970) and as long as three minutes (FAA, 2002). Wake vortex encounters pose a severe hazard to trailing aircraft, especially when the trailing aircraft are smaller in size (McGowan, 1968). Flying in close proximity to the airport runway increases the level of hazard because the wake vortex circulation is at a maximum (Arndt et al., 1991). Wake vortex and turbulence generated by large aircraft is strong and can be unsafe to trailing aircraft (Ortega et al., 2002).

The spacing between aircraft within the take-off and landing corridors at busy airports is maintained according to the International Civil Aviation Organization's (ICAO's) Weight Class Dependent Separation Criteria (Elsenaar, 2006). The separation criteria are used to avoid trailing aircraft experiencing strong swirling flows. At present, aircraft segregation is based on an overly conservative basis due to an uncertainty in knowing the location of the vortices relative to the flight path (Babie and Nelson, 2004) and hence, allows far more separation distance between aircraft than is really needed to avoid accidents. However, the financial repercussions of these separation requirements are staggering (Matalanis and Eaton, 2007).

Naturally, wake vortices are very slow to dissipate and therefore methods of increasing the dissipation rate have to be studied. Multiple vortex pair systems (co-rotating and counter-rotating vortices) have been studied as vortex modification concepts to produce weaker wakes (Fabre et al., 2002; Durston et al., 2005; Savas, 2005).

Particle Image Velocimetry was used to test the technique of differential spoiler setting (DSS) in a scaled half-model aircraft to characterize the generated wake vortices in the near wake field (Elsayed et al., 2010, 2011). The core radius of the

merged vortex had increased by a factor of up to 2.72, relative to the undisturbed flap tip vortex and a 44% decrease in the maximum cross-flow velocity was witnessed for the case of deployed spoilers, relative to undisturbed flap tip vortex maximum cross-flow velocity. Numerical results were in agreement with the experimental results (Ludin et al., 2013).

Several investigations have been conducted with add-on devices to modify the vortex rollup process and to instil a fast growing instability in the wake of an aircraft such that the resultant vortex is more diffused. A spoiler mounted on the wing tip (Corsiglia et al., 1971), splines mounted downstream of the wing tip (Patterson, 1975), spoilers of delta type plan-form deployed in the area of the outboard flap (Breitsamter, 2011), a tip-mounted slender half delta wing (Lee and Pereira, 2013) and a tip-mounted reverse half delta wing (Lee and Su, 2012) are a few examples of experiments conducted with add-on devices.

Recent investigations indicate that reverse delta type add-on devices may have the capability to be used in wake vortex alleviation (Coustals et al., 2006; Altaf et al., 2011, 2016). Vortices produced by a reverse delta type add-on device may introduce a fast growing instability (countersign vorticity) into the wake and modify the vortex roll up process. Interaction of the vortices may create a weaker resultant vortex with a reduction in peak vorticity, peak tangential velocity and core circulation. A more diffused resultant vortex is expected which can enhance wake vortex decay and thus, lead to wake vortex alleviation.

Particle Image Velocimetry (PIV) studies of add-on devices for the purpose of wake vortex alleviation are limited. This particular study of a reverse delta type add-on device is one such endeavour in attempting to minimize the wake vortex hazard posed on trailing aircraft.

PIV, a minimally intrusive method, is used to study the characteristics of the vortex interactions of vortices created by a reverse delta type add-on device and the flap-tip of a half-span wing model. Resultant vortex characteristics such as core radius, maximum tangential velocity and vorticity are presented.

Method

The closed-loop low-speed wind tunnel at International Islamic University Malaysia (IIUM) was used to conduct the experiments. The maximum achievable velocity in the wind tunnel is 50 m/s. The dimensions of the wind tunnel test section are 6.00 m (length) by 2.30 m (width) by 1.50 m (height). The wind tunnel has a free-stream turbulence intensity of 0.07% in the flow direction, 0.10% in the lateral

direction and 0.11% in the vertical direction.

The model attachment point on the IIUM wind tunnel floor is at the centre of the test section. Therefore, the farthest region at which the PIV CCD (charge coupled device) camera could be placed was approximately 3 metres downstream of the half-span wing model. The farthest achievable PIV measurement region in the wind tunnel was approximately 2.20 metres from the half-span wing model. The test section floor is fitted with a turntable which was used to make the model's angle of attack variations. A major limitation of small wind tunnels, such as in this study, is the inability to conduct far field wake studies.

The CCD camera was placed in the flow stream at a distance of 2 to 3 mean chord lengths downstream of the measurement plane resulting in minimal disturbance to the upstream flow. Zhang et al. (2006) found that once the distance between the measurement plane and a blunt object placed in the wind tunnel exceeds 2 mean chords of the experimental model, the influence of the blunt object on the flow in the measurement plane was less than 5% on the scattering of vortex centres and less than 2% on maximum vorticity. Therefore, for this study, it can be concluded that the effect of the CCD camera on the flow is considered to be insignificant as it is more than 3 mean chords away from the measurement plane.

Model

The half-span wing model used in this work consists of a wing with a tapered NACA 23012 profile and is tested at landing configuration/High Lift Configuration (slat extension 15° and flap extension 20°), shown in Fig. 1. Two sets of reverse delta type add-on devices are used for this work, namely Small reverse delta type add-on device (S-rdw) and Large reverse delta type add-on device (L-rdw), shown in Fig. 2. The reverse delta type add-on devices have a thickness of 3 mm, sweep angle 69.4° and bevel angle of 20° . The reverse delta type add-on devices are attached to the main wing by a 35 mm long adjustable mounting which is used to make angle of attack variations. The reverse delta type add-on device is to be extended using hydraulic systems and to be used only during the take-off and landing phase of flight. For rest of the flight envelope, the add-on device is to be retracted and stowed in the main wing.

Procedure

Velocity components at four downstream planes perpendicular to the stream-wise direction are investigated; $x/(b/2) = 0.021, 0.548, 1.075$ and 2.387 , where x is the stream-wise coordinate and b is the wing span length. The schematic diagram

of the experimental setup is shown in Fig. 3. Four downstream planes are chosen so that the flow characteristics can be differentiated in terms of roll up, vortex core size, tangential velocity and vorticity.

A free stream velocity (V_∞) of 12 m/s corresponding to an average chord based Reynolds Number of $Re_c = 2.75 \times 10^5$ was used. Tracer particles of a mean diameter of 1 μm were injected into the wind tunnel test section using a fog generator. The time interval between image frames was fixed to 60 μs and the laser sheet thickness was fixed to 2 mm. To illuminate the flow, a light sheet from a neodymium-doped yttrium aluminium garnet (Nd:YAG) laser system of wavelength 532 nm was used. A CCD camera was placed perpendicular to the laser sheet, downstream of the half-span wing to capture the motion of tracer particles.

PIV data was obtained for High Lift Configuration (HLC) at $\alpha=7.7^\circ$ and HLC with reverse delta type add-on devices at $\alpha=9.7^\circ$, where α is the angle of attack of the half-span wing. A target lift coefficient $C_L=1.06$ is achieved for HLC at an angle of attack 7.7° and velocity 12 m/s. Due to the addition of an add-on device to the half-span wing at HLC, it was anticipated that increasing the half-span wing model angle of attack by 1° - 2° will recover the target lift coefficient that was achieved at HLC without an add-on device. Therefore, the half-span wing model with the add-on device was tested at $\alpha=9.7^\circ$.

The angle of attack of the reverse delta type add-on device was fixed at $\alpha_{rdw}=+30^\circ$. Tests were also performed for $\alpha_{rdw}= \pm 20^\circ$ and $+30^\circ$ but the most favourable case of $\alpha_{rdw}= +30^\circ$ was chosen for investigation. 100 PIV images were recorded for each case and post-processed using adaptive correlation with a 25% overlap. The 100 PIV vector maps were averaged to estimate the mean velocity in the region of focus. An interrogation area size of 32×32 pixels is used which yields 66×49 vectors per image. The measurement resolution is 1600×1186 pixels and the time between recordings is 1 second.

Results

Velocity Vectors and Vorticity Contours

Vortices are very slow to dissipate naturally and may take several kilometres to dissipate downstream of a large aircraft. Vortex dissipation rate can be accelerated if the vortex core dimension is increased significantly by using vortex modification techniques such as using wing devices that can alter the vortex rollup process. A more diffused vortex core at the same downstream location implies a weaker vortex (National Research Council, 2008).

The add-on device is likely to significantly increase the resultant vortex core dimension which lowers the vortex strength and increases the vortex dissipation rate. Using the International Organization for Standardization (ISO) procedure, an uncertainty analysis of the PIV velocity measurements was performed (Figliola and Beasley, 1995). Based on 95% confidence intervals, the total uncertainty in velocity was found to be ± 0.188 m/s.

Figures 4 to 7 show the velocity vectors of a half-span wing model at HLC with/without a reverse delta type add-on device attached near the half-span wing model outboard flap-tip at $x/(b/2) = 0.021, 0.548, 1.075$ and 2.387 . This investigation was carried out to determine if the resultant vortex formed after the merging of the reverse delta type add-on device vortices and the flap-tip vortex yields a more diffused vortex.

Figures 4a, 5a, 6a and 7a show the velocity vectors, tangential velocity magnitude (V_θ) and vorticity contours of the HLC flap-tip vortex. It is observable that the flap-tip vortex is not very strong. This is because the flap deflection is set to $\delta = 20^\circ$ only and the flap is a single element flap. It is clearly noticeable that the flap-tip vortex is well rolled up at downstream plane $x/(b/2) = 0.548$ but the vortex rollup is weaker (less compact vortex) at farther downstream planes. The tangential velocity magnitude is seen to decrease slightly between downstream planes. Reynolds (1876) attributed the reduction in the tangential velocity to the growth of the vortex in order to conserve momentum. As the vortex propagates through the fluid its volume increases with time due to the entrainment of the surrounding fluid.

The flap-tip vortex of the HLC without the add-on device exhibits a better rollup than the HLC with the add-on device, as shown in figures 5a, 6a and 7a. The flap-tip vortex of the HLC has diffused (enlarged) from $x/(b/2) = 0.548$ to $x/(b/2) = 1.075$ by 12.1% and from $x/(b/2) = 1.075$ to $x/(b/2) = 2.387$ by 20.8%. This increase in vortex core radius within 2 half-span lengths is significantly high. This indicates that the flap-tip vortex of the HLC is not very strong and hence, it has significantly diffused without any instabilities being introduced.

When the reverse delta type add-on device is used, as shown in figures 5b-c, 6b-c and 7b-c, the vortex core radius is found to have diffused more than the case without an add-on device. At $x/(b/2) = 0.548$, the resultant flap-tip vortex core radius compared to the case without an add-on device has increased by 24.9% and 31.9% for the Small reverse delta type add-on device (S-rdw) case and Large reverse delta type add-on device (L-rdw) case, respectively. At $x/(b/2) = 1.075$, the resultant flap-tip vortex core radius compared to the case without an add-on device has increased

by 22.6% and 37% for the S-rdw case and L-rdw case, respectively. At $x/(b/2)=2.387$, the resultant vortex core radius compared to the flap-tip vortex core radius of the HLC has increased by 19.8% and 33.4% for the S-rdw case and L-rdw case, respectively. The results suggest that the weak flap-tip vortex of the HLC is diffusing significantly.

When an add-on device is used, the resultant flap-tip vortex core size increases significantly more than the HLC flap-tip vortex. The significant increase in resultant flap-tip vortex core radius indicates that the reverse delta type add-on device is capable of alleviating wake vortex strength.

When a reverse delta type add-on device is used, as shown in figures 5b-c, 6b-c and 7b-c, the tangential velocity magnitude of the resultant vortex is seen to decrease slightly with respect to the HLC flap-tip vortex. The maximum tangential velocity reduction recorded between downstream plane 2 and downstream plane 4 for the HLC was 19.6%. The maximum tangential velocity reduction for the S-rdw case and the L-rdw case compared to the HLC case was 29.3% and 36.1%, respectively. This significant reduction in tangential velocity magnitude is indicative of flap-tip vortex breakdown and more rapid diffusion of the resultant flap-tip vortex. It can be said that the add-on device creates small scale instabilities into the flap-tip vortex causing the resultant flap-tip vortex to breakdown significantly. The weaker resultant flap-tip vortex diffuses more rapidly.

For all investigated cases, the vorticity decreased gradually from a maximum at the centre to nearly zero at the outer region of the vortices. At $x/(b/2)=0.021$, closer vorticity contours at the centre of the vortex are recorded, as shown in figures 4a-c. It can be noticed that the vortex cores are distinguishable. At $x/(b/2)=0.548$, the vortex core for the HLC only is distinguishable (see Appendix figure a), whereas the vorticity contours for the add-on device cases (see Appendix figures 5b-c) are broken into small vorticity patches. These small patches of vorticity have high individual vorticity magnitudes but they do not pose a hazard as they are too small to cause any significant circulation of the entire vortex core. At farther downstream locations, the small vorticity patches increase in number for the add-on device cases. This indicates that the vortex core is mostly broken down.

The breakdown of the resultant flap-tip vortex creates a weaker and more diffused/scattered/distributed vortex. Hazard from such vortices is minimal. A rapidly diffusing vortex rejects vorticity from the vortex core. The rejection of vorticity reduces the circulation of the vortex and its strength (Maxworthy, 1972). For the HLC, the vortex core is only largely diffused at $x/(b/2)=2.387$. Thus, it can be said that when the add-on device is used, the resultant vortex formed breaks

down rapidly due to small scale instabilities created into the vortex. The weak resultant flap-tip vortex diffuses significantly more than the HLC case.

Direct interaction of the vortices generated by the add-on device with the flap-tip vortex creates a resultant vortex with a weaker rollup, lower tangential velocity and larger vortex core. The vortex system with co-rotating and counter-rotating vortices experiences a lower tangential velocity due to instabilities created by the direct interaction of the co-rotating and counter-rotating vortices within the vortex system which lead to a breakdown of the resultant flap-tip vortex causing rapid diffusion of the weaker resultant flap-tip vortex (Coustols et al., 2006).

Also, the flap-tip vortex and the reverse delta type add-on device vortex in close proximity of the flap-tip are co-rotating vortices, as shown in figures 4b-c. These co-rotating vortices are very close to each other and at the point where the vortices meet; they have opposite direction of rotation. There is also a counter rotating vortex of the reverse delta type add-on device present. The interactions between these three vortices lower the tangential velocity magnitude of the resultant flap-tip vortex and cause it to breakdown and diffuse more rapidly than the HLC case, as shown in figures 5-7 (see Appendix). It can be concluded that the use of a reverse delta type add-on device causes the resultant vortex to diffuse more rapidly.

Aerodynamic Performance

The six-component force balance in the IIUM closed loop low-speed wind tunnel was used to obtain the aerodynamic performance of the half-span wing model with/without the reverse delta type add-on devices. Also, the aerodynamic performance of the plain wing configuration (slat extension 0° and flap extension 0°) was obtained.

Figure 8a shows the lift coefficient (C_L) and the moment coefficient (C_m) curves of all the cases studied. HLC exhibits the highest lift coefficient at $\alpha=18^\circ$ and it stalls between $\alpha=18^\circ$ and $\alpha=19^\circ$. The S-rdw and L-rdw configurations stall between $\alpha=19^\circ$ and $\alpha=20^\circ$. This is an advantageous phenomenon which allows the stall of the wing to be delayed by 1° by using an add-on device. This happens because the air between the add-on device and the main wing is accelerated and delays the separation of the flow over the main wing. The lift coefficient curves are nearly identical until $\alpha=0^\circ$ and then diverge slowly beyond that. The reduction in the lift coefficient values between the HLC, S-rdw and L-rdw cases is 3.8%. The moment coefficient curves show that the stability of the wing is maintained for all investigated cases.

Figure 8b shows the drag coefficient (C_D) curves for all cases studied. The drag increment (compared with the HLC drag coefficient as the base value at target lift coefficient) for S-rdw case is 7.7% and for L-rdw case is 14.9%. To maintain the target lift coefficient, it was found that an increase of 1.0° in the angle of attack of the half-span wing is required to compensate for the reduction of lift when the add-on device is used. The increase of 1.0° in angle of attack causes a 6.2% increase in drag. The overall findings of the investigation are listed in Table 1.

Table 1
Overall findings of the investigation

Vortex Core Size	Tangential Velocity	Lift Coefficient	Drag Coefficient
+37% (factor of 1.37)	-36.1%	-3.8%	+14.9%

'+' indicates increase '-' indicates decrease

Conclusion

PIV was used to study the vortex structures of a half-span wing with a reverse delta type add-on device attached in the proximity of the outboard flap-tip at High Lift Configuration. It was found that the resultant vortex core radius has increased, its vorticity magnitude has decreased and its tangential velocity magnitude has decreased significantly compared to the flap-tip vortex at HLC. The resultant vortex core radius has increased by 37% compared to the HLC. Between downstream plane 2 and 4, the maximum tangential velocity reduction recorded for the HLC was 19.6%, whereas the maximum tangential velocity reduction for the S-rdw case and the L-rdw case compared to the HLC case was 29.3% and 36.1%, respectively. The use of a reverse delta type add-on device causes the resultant vortex core to breakdown significantly whereas the vortex core of the HLC is still relatively intact, as can be seen from the vorticity contours.

L-rdw case is more favourable as the tangential velocity magnitude recorded is lower, the resultant vortex core radius is larger (more diffused) and the vorticity core is more disintegrated than the S-rdw case and the HLC case. The use of a reverse delta type add-on device moderately adversely affects the aerodynamic performance of the half-span wing model. The lift coefficient reduction is 3.8% and the drag coefficient increment is 14.9%. From the above observations, it can be concluded that usage of a reverse delta type add-on device has several benefits.

References

- Altaf, A., Omar, A. A., Asrar, W. and Ludin, H. B. (2011). A study of the reverse delta wing. *Journal of Aircraft*, 48(1), 277-286. Doi: 10.2514/1.C031101
- Altaf, A., Thong, T. B., Omar, A. A. and Asrar, W. (2016). Influence of a reverse delta type add-on device on wake vortex alleviation. *AIAA Journal*, 54(2), 625-636. DOI: 10.2514/1.J054436.
- Andrews, W. H. (1970). Flight evaluation of the wing vortex wake generated by large jet transports. In: *Aircraft wake turbulence and its detection* (pp 287-288). New York: Springer US. Doi: 10.1007/978-1-4684-8346-8_17
- Arndt, R.E.A., Arakeri, V.H. and Higuchi, H. (1991). Some observations of tip vortex cavitation. *Journal of Fluid Mechanics*, 229, 269-289. Doi: 10.1017/S0022112091003026
- Babie, B. M. and Nelson, R. C. (2004). Flow Visualization Study of Far Field Wake Vortex Interactions. *11th International Symposium on Flow Visualization*. Indiana: University of Notre Dame.
- Breitsamter, C. (2011). Wake vortex characteristics of transport aircraft. *Progress in Aerospace Sciences*, 47(2), 89-134. Doi: 10.1016/j.paerosci.2010.09.002
- Corsiglia, V. R., Jacobsen, R. A. and Chigier, N. (1971). An experimental investigation of trailing vortices behind a wing with a vortex dissipater. In: *Aircraft wake turbulence and its detection* (pp 229-242). New York: Springer US. Doi: 10.1007/978-1-4684-8346-8_14
- Coustols, E. (2006). An overview of European projects on wake vortices. Proceedings of the workshop on *Principles of wake vortex alleviation devices*. France: ONERA Toulouse.
- Coustols, E., Jacquin, L. and Shrauf, G. (2006). Status of wake vortex alleviation in the frame work of European collaboration: validation attempts using tests and CFD results. *ECCOMAS CFD* conference. The Netherlands: Technical University of Delft.
- Durston, D. A., Walker, S. M., Driver, D. M., Smith, S. C. and Savas, O. (2005). Wake-vortex alleviation flowfield studies. *Journal of Aircraft*, 47(4), 894-907. Doi: 10.2514/1.7904

- Elsayed, O. A., Asrar, W., Omar, A. A., and Kwon, K. (2010). Influence of Differential Spoiler Settings on the wake vortex characterization and alleviation. *Journal of Aircraft*, 47(5), 1728-1738. Doi: 10.2514/1.C000258
- Elsayed, O. A., Asrar, W., Omar, A. A., and Kwon, K. (2011). Effect of Differential Spoiler Settings (DSS) on the Wake Vortices of a Wing at High-Lift-Configuration (HLC). *Journal of Aerospace Science and Technology*, 15(7), 555-566. Doi:10.1016/j.ast.2010.11.001
- Elsenaar, B. (2006). Improved wake vortex separation ruling and reduced wake signatures. *WakeNet2-Europe in collaboration with WakeNet-USA*, 1, 1-51. Doi: 10.1016/j.ast.2007.09.008
- FAA (2002). *Air traffic control*. Order 7110.65N
- Fabre, D., Jacquin, L., and Loof, A. (2002). Optimal perturbations in a four-vortex aircraft wake in counter-rotating configuration. *Journal of Fluid Mechanics*, 451, 319-328. Doi: 10.1017/S0022112001006954
- Figliola, R. S., and Beasley, D. E. (1995). *Theory and Design for Mechanical Measurements*. Singapore: Wiley.
- Lee, T. and Pereira, J. (2013). Modification of static-wing tip vortex via a slender half-delta wing. *Journal of Fluids and Structures*, 43, 1-14. Doi: 10.1016/j.jfluidstructs.2013.08.004
- Lee, T. and Su, Y. Y. (2012). Wingtip vortex control via the use of a reverse half delta wing. *Experiments in Fluids*, 52(6), 1593-1609. Doi: 10.1007/s00348-012-1274-8.
- Ludin, H. B., Omar, A. A. and Asrar, W. (2013). Numerical Study of the Effect of Spoiler Configuration on Wake Vortex Alleviation. *Journal of Aerospace Engineering*, 28(3). Doi: 10.1061/(ASCE)AS.1943-5525.0000406
- Matalanis, C. G. and Eaton, J. K. (2007). Wake vortex alleviation using rapidly actuated segmented gurney flaps. *The Stanford Thermal and Fluid Sciences Affiliates and the Office of Naval Research*. Stanford: Stanford University.
- Maxworthy, T. (1972). The structure and stability of vortex rings. *Journal of Fluid Mechanics*, 51, 15-32. Doi: 10.1017/S0022112072001041

- McGowan, W. A. (1968). Trailing vortex hazard. *SAE Technical Paper 680220*.
Doi: 10.4271/680220.
- National Research Council (2008). *Wake Turbulence: An Obstacle to Increased Air Traffic Capacity*. Washington D.C.: National Academies Press.
- Ortega, J. M., Bristol, R. L. and Savas, O. (2002). Wake alleviation properties of triangular-flapped wings. *AIAA Journal*, 40(4), 709–721. Doi: 10.2514/2.1703
- Patterson, J. C. (1975). Vortex attenuation obtained in the langley vortex research facility. *Journal of Aircraft*, 12(9), 745-749. Doi: 10.2514/3.59865
- Reynolds, O. (1876). On the resistance encountered by vortex rings and relation between the vortex rings and the streamlines of a disk. *Nature*, 14, 477-479.
- Savas, O. (2005). Experimental investigations on wake vortices and their alleviation. *Academie des Sciences*, 6(4-5), 415-429. Doi: 10.1016/j.crhy.2005.05.004
- Veillette, P. R. (2002). Data show that U.S. wake-turbulence accidents are most frequent at low altitude and during approach and landing. *Flight Safety Digest*, 21(3-4), 1-56.
- Zhang H. J., Zhou, Y. and Whitelaw, J. H. (2006). Near field wing-tip vortices and exponential vortex solution. *Journal of Aircraft*, 43(2), 445-449. Doi: 10.2514/1.15938

Appendix

Figure 1. Schematic of the Half-Span Wing model with a large reverse delta type add-on device attached. Dimensions are in millimetres (mm).

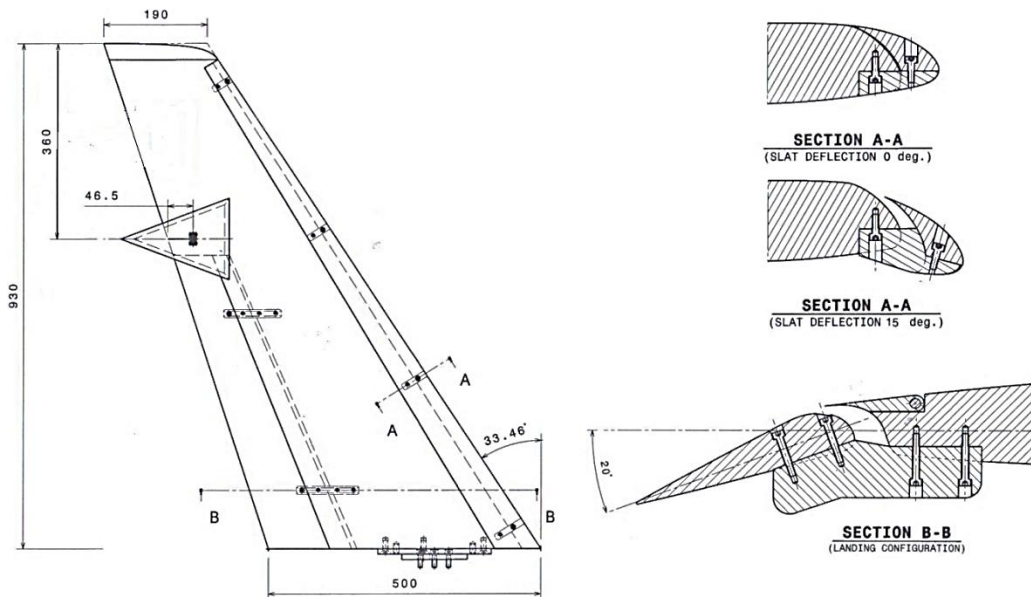


Figure 2. Schematic of the reverse delta type add-on devices (from left: small rdw add-on device (S-rdw) and large rdw add-on device (L-rdw)). Dimensions are in millimetres (mm).

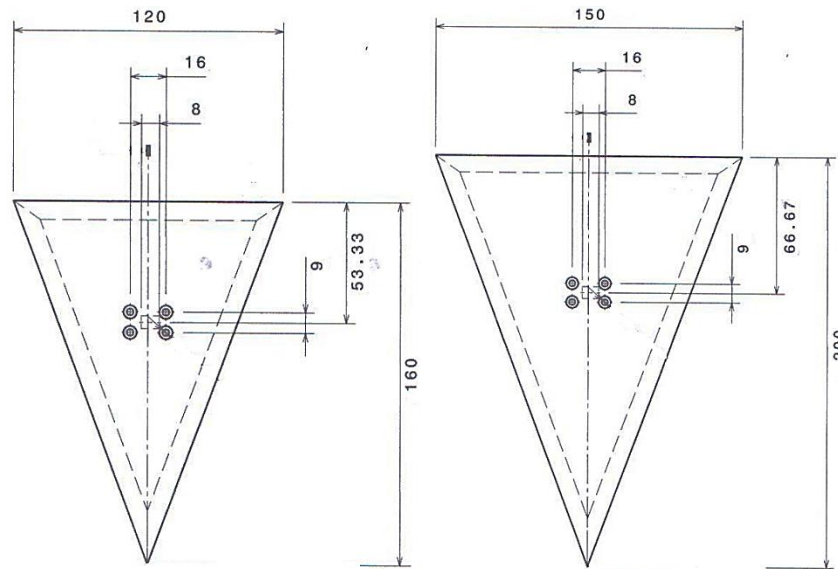


Figure 3. Schematic of the experimental setup

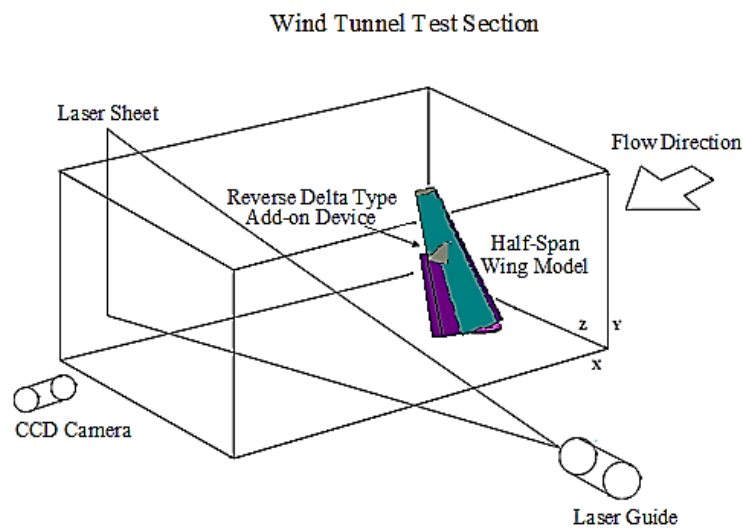
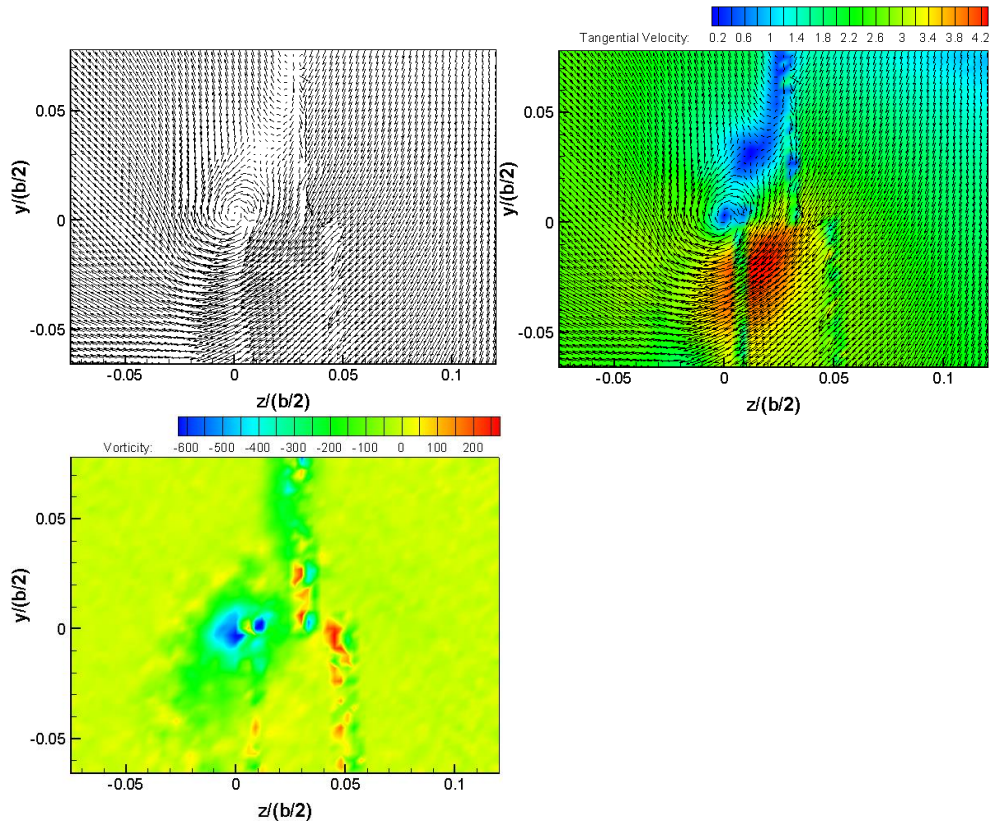
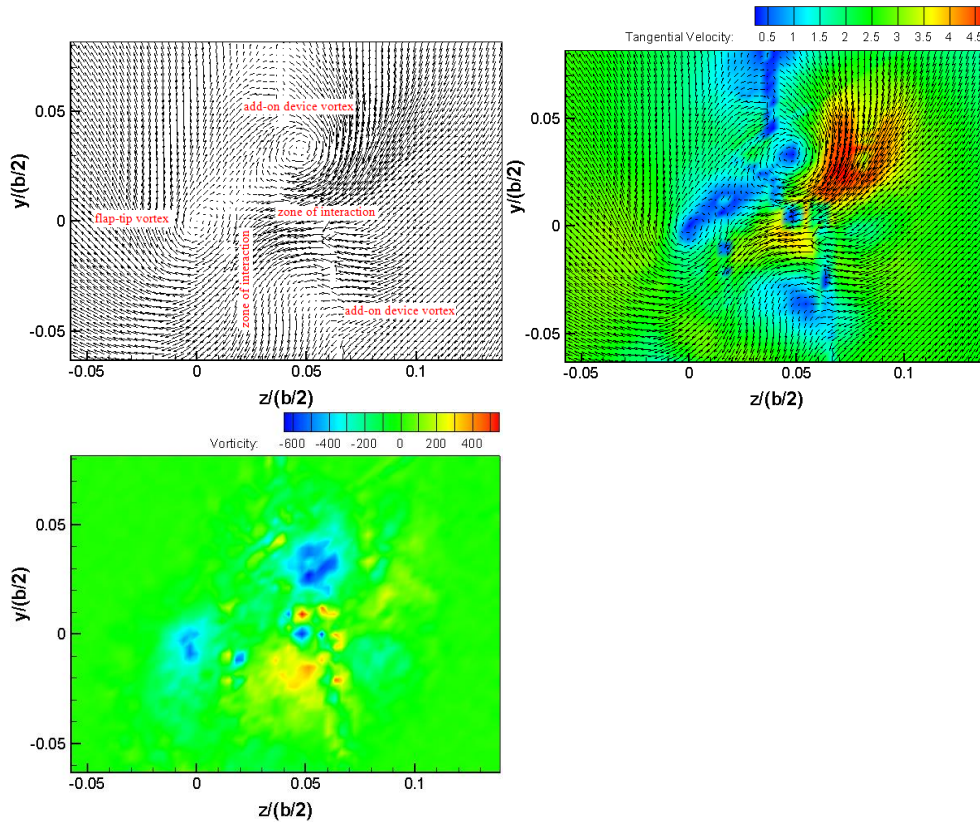


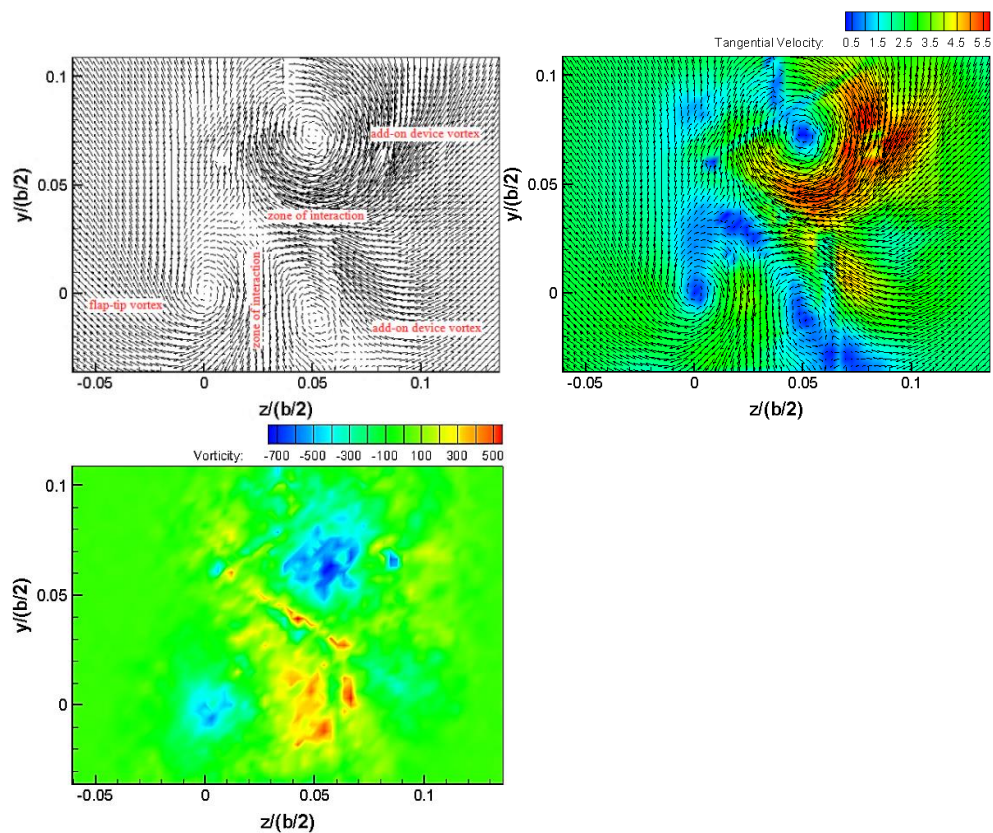
Figure 4. Velocity Vectors, Tangential Velocity Magnitude and Vorticity Contours at $x/(b/2)=0.021$ for (a) High Lift Configuration $\alpha=7.7^\circ$, (b) High Lift Configuration $\alpha=9.7^\circ$ with S-rdw add-on device ($\alpha_{S\text{-rdw}}=+30^\circ$) and (c) High Lift Configuration $\alpha=9.7^\circ$ with L-rdw add-on device ($\alpha_{L\text{-rdw}}=+30^\circ$)



a) High Lift Configuration case, $\alpha=7.7^\circ$, $x/(b/2)=0.021$, $V_\infty=12$ m/s.

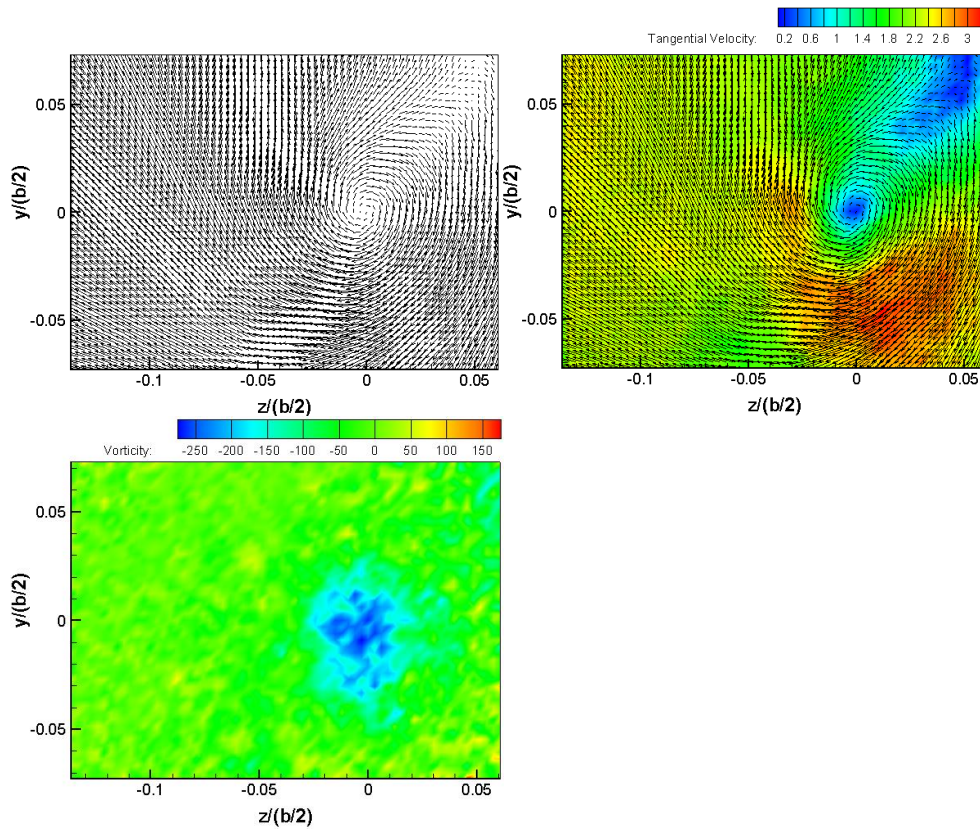


b) High Lift Configuration case, $\alpha=9.7^\circ$; with S-rdw add-on device, $\alpha_{S-rdw}= +30^\circ$, $x/(b/2)=0.021$, $V_\infty=12$ m/s.

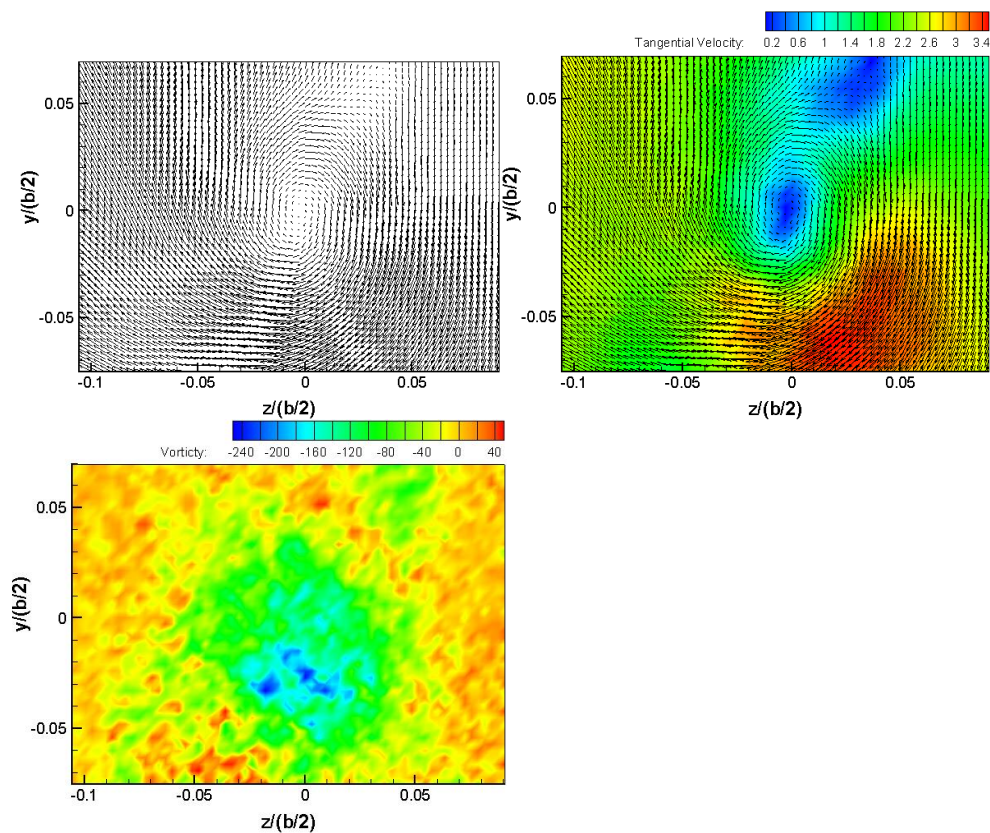


c) High Lift Configuration case, $\alpha=9.7^\circ$; with L-rdw add-on device, $\alpha_{Lrdw}=+30^\circ$,
 $x/(b/2)=0.021$, $V_\infty=12$ m/s.

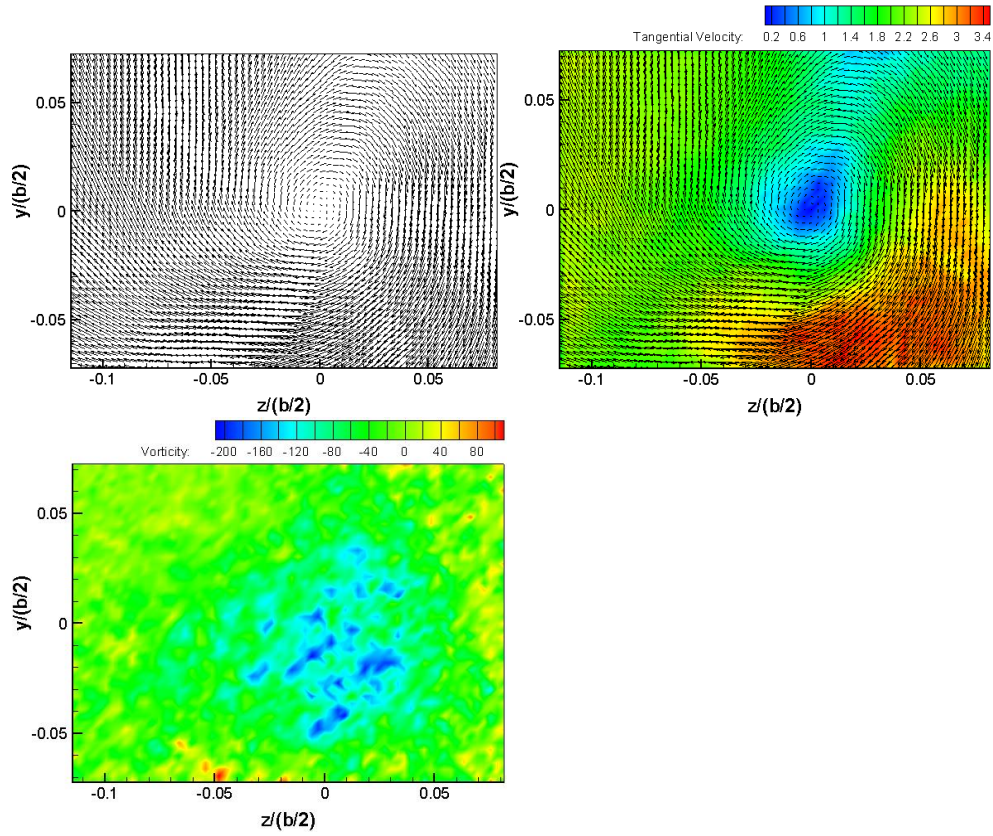
Figure 5. Velocity Vectors, Tangential Velocity Magnitude and Vorticity Contours at $x/(b/2)=0.548$ for (a) High Lift Configuration $\alpha=7.7^\circ$, (b) High Lift Configuration $\alpha=9.7^\circ$ with S-rdw add-on device ($\alpha_{S-rdw}=+30^\circ$) and (c) High Lift Configuration $\alpha=9.7^\circ$ with L-rdw add-on device ($\alpha_{L-rdw}=+30^\circ$)



a) High Lift Configuration case, $\alpha=7.7^\circ$, $x/(b/2)=0.548$, $V_\infty=12$ m/s.

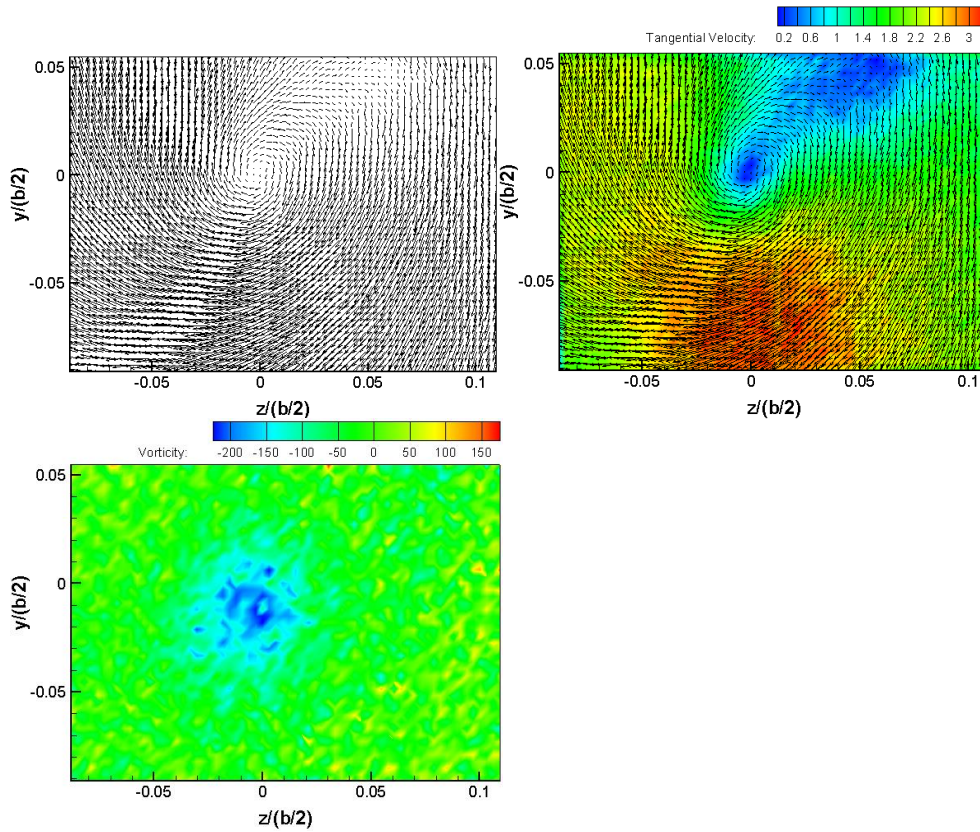


b) High Lift Configuration case, $\alpha=9.7^\circ$; with S-rdw add-on device, $\alpha_{S-rdw}=+30^\circ$,
 $x/(b/2)=0.548$, $V_\infty=12$ m/s.

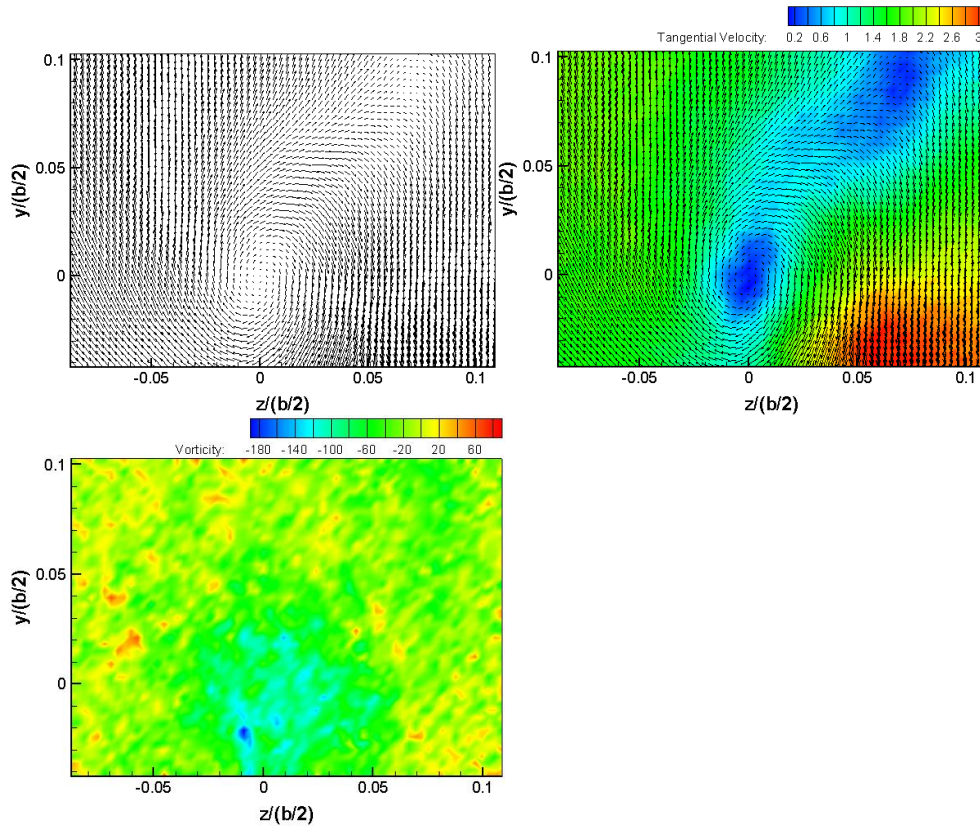


c) High Lift Configuration case, $\alpha=9.7^\circ$; with L-rdw add-on device, $\alpha_{Lrdw}=+30^\circ$,
 $x/(b/2)=0.548$, $V_\infty=12$ m/s.

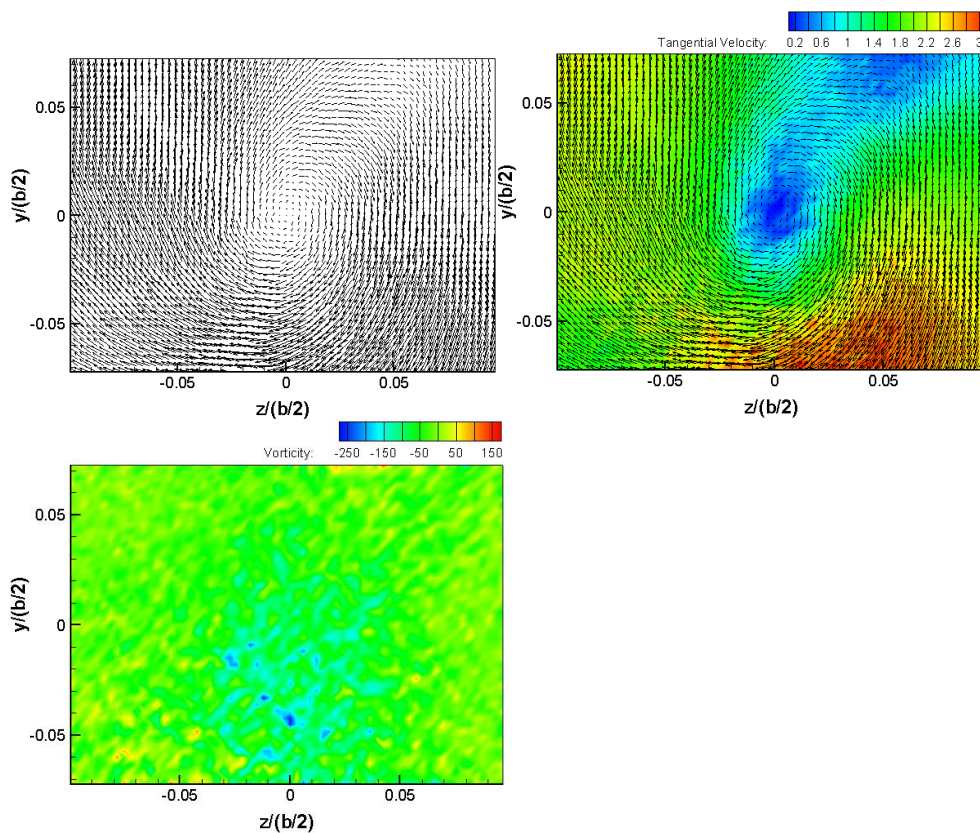
Figure 6. Velocity Vectors, Tangential Velocity Magnitude and Vorticity Contours at $x/(b/2)=1.075$ for (a) High Lift Configuration $\alpha=7.7^\circ$, (b) High Lift Configuration $\alpha=9.7^\circ$ with S-rdw add-on device ($\alpha_{S\text{-rdw}}=+30^\circ$) and (c) High Lift Configuration $\alpha=9.7^\circ$ with L-rdw add-on device ($\alpha_{L\text{-rdw}}=+30^\circ$)



a) High Lift Configuration case, $\alpha=7.7^\circ$, $x/(b/2)=1.075$, $V_\infty=12$ m/s.

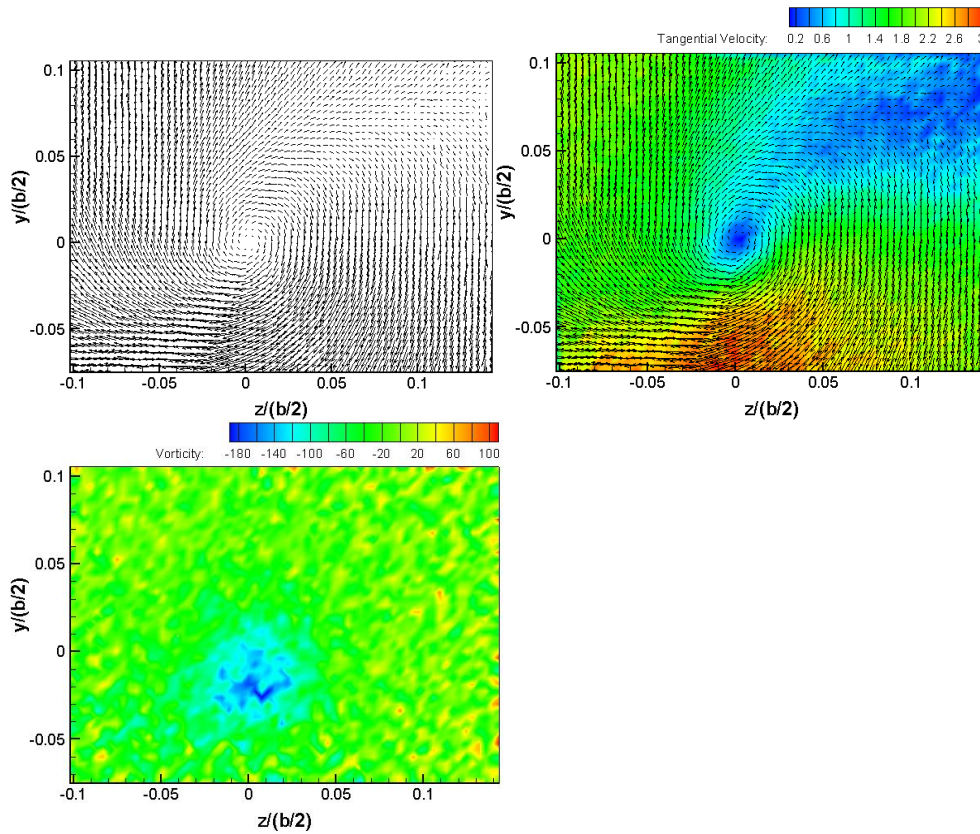


b) High Lift Configuration case, $\alpha=9.7^\circ$; with S-rdw add-on device, $\alpha_{S-rdw}=+30^\circ$, $x/(b/2)=1.075$, $V_\infty=12$ m/s.

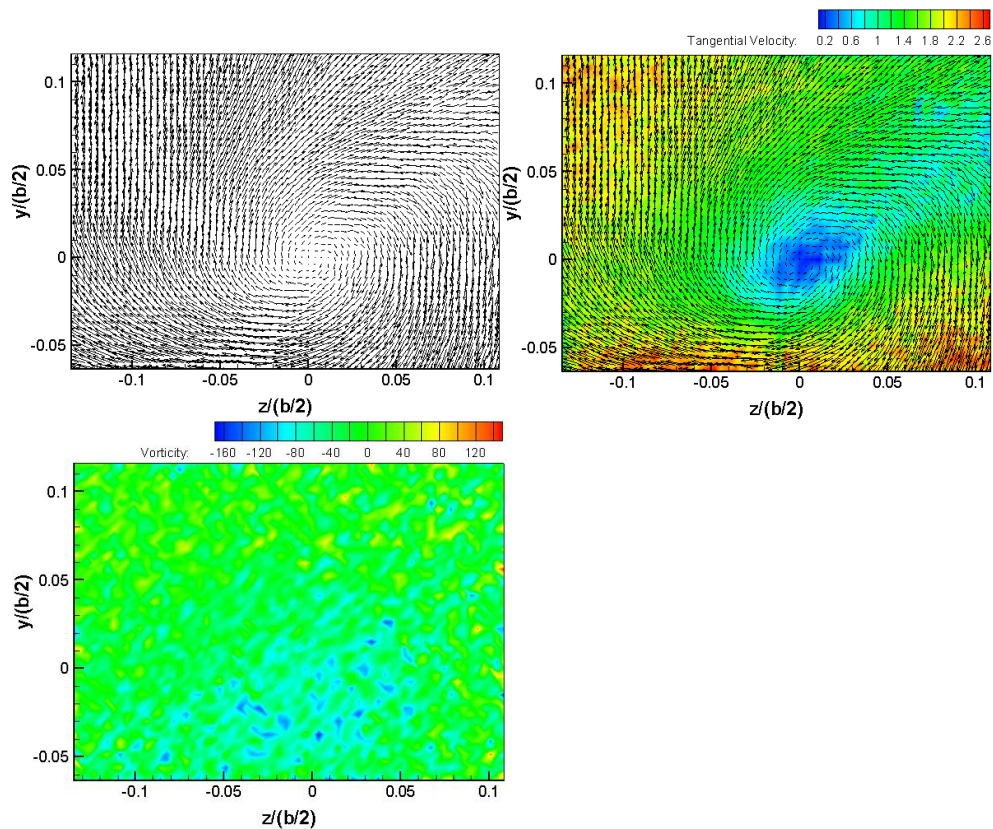


c) High Lift Configuration case, $\alpha=9.7^\circ$; with L-rdw add-on device, $\alpha_{Lrdw}=+30^\circ$,
 $x/(b/2)=1.075$, $V_\infty=12$ m/s.

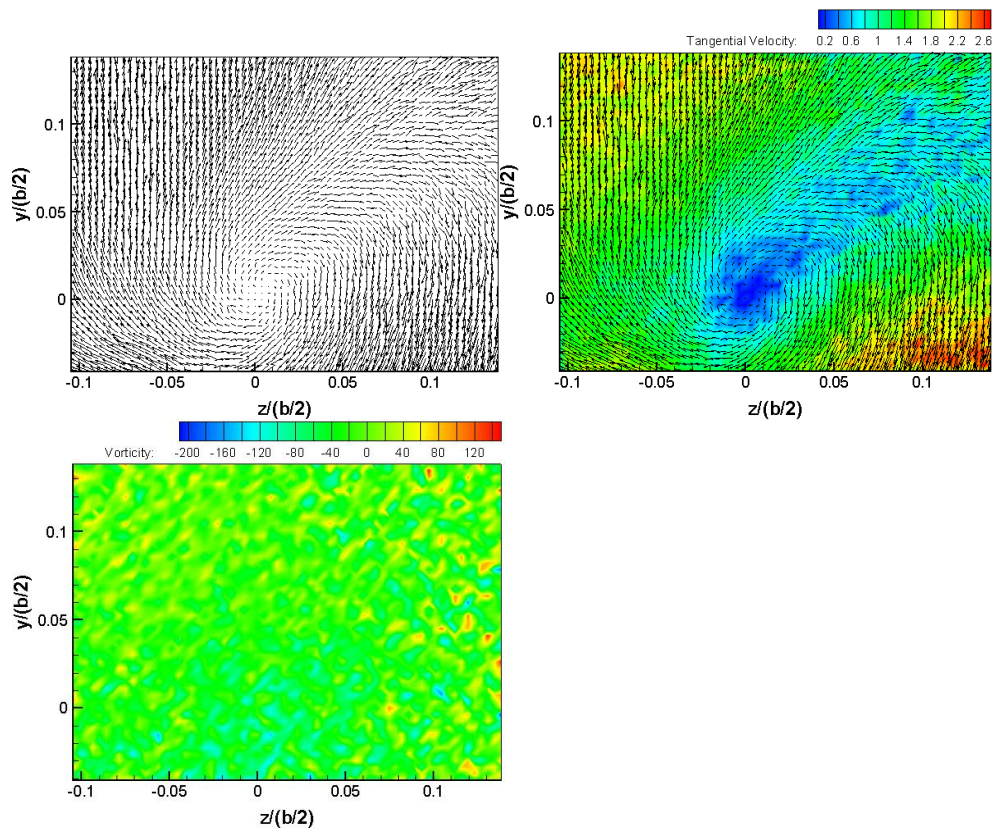
Figure 7. Velocity Vectors, Tangential Velocity Magnitude and Vorticity Contours at $x/(b/2)=2.387$ for (a) High Lift Configuration $\alpha=7.7^\circ$, (b) High Lift Configuration $\alpha=9.7^\circ$ with S-rdw add-on device ($\alpha_{S\text{-rdw}}=+30^\circ$) and (c) High Lift Configuration $\alpha=9.7^\circ$ with L-rdw add-on device ($\alpha_{L\text{-rdw}}=+30^\circ$)



a) High Lift Configuration case, $\alpha=7.7^\circ$, $x/(b/2)=2.387$, $V_\infty=12$ m/s.



b) High Lift Configuration case, $\alpha=9.7^\circ$; with S-rdw add-on device, $\alpha_{S-rdw}=+30^\circ$, $x/(b/2)=2.387$, $V_\infty=12$ m/s.



c) High Lift Configuration case, $\alpha=9.7^\circ$; with L-rdw add-on device, $\alpha_{Lrdw}=+30^\circ$,
 $x/(b/2)=2.387$, $V_\infty=12$ m/s.

Figure 8. Aerodynamic performance of the Plain Wing, HLC, HLC with S-rdw and HLC with L-rdw

